ARC Geophysical Research

Thermodynamically Constrained Averaging Theory: Why Bother?

Timothy M. Weigand [*1], William G. Gray [1,2], and Cass T. Miller [1]

[1]University of North Carolina, Chapel Hill
[2]University of Vermont

Abstract

Porous medium researchers and practitioners usually rely on macroscale models to represent systems of concern. While macroscale models have often been formulated phenomenologically, the thermodynamically constrained averaging theory (TCAT) provides a means to rigorously derive closed macroscale models for a wide variety of systems. However, the TCAT approach can appear overwhelmingly complicated, the entry point for use unclear, and the advantages are not self-evident. In response to these perceived shortcomings, we demonstrate several aspects of TCAT macroscale model formulations for single-fluid flow in a porous medium. Specifically, we illustrate an essentially exact macroscale model derived from a rigorous connection across scales, show how an entropy inequality can be used to derive an approximate macroscale form for the Stokes-flow regime, and examine models in the transition-flow regime. A special emphasis is placed upon leveraging available results, and other application opportunities are discussed.

Keywords: Model Development, Upscaling, Porous Media

1 Introduction

Porous medium systems are usually modeled mechanistically at a continuum scale for which upscaling or averaging has been performed, or assumed phenomenologically to have been performed, such that phase boundaries are not resolved and the state is represented in part by extent measures, such as porosity, volume fractions, and saturations [4]. This scale will be

*Corresponding Author
E-mail addresses: timothy.weigand@unc.edu
doi: https://doi.org/10.5149/ARC-GR.1362

referred to as the macroscale, although this terminology is not universally used in the literature. Macroscale models are historically, and frequently still, posited phenomenologically [5, 18]. Phenomenological models are so ingrained in porous medium research and practice that they are accepted nearly universally within the hydrological community. These mechanistic models include some combination of conservation equations and closure relations, which are needed to render a model mathematically solvable. Without question, this approach has led to descriptions that have benefited society and are widely accepted; many would consider traditional phenomenological models of porous medium systems to be settled science.

A growing research community has also developed in the area of microscale, or porescale, modeling with boundaries between phases resolved in space and time [9, 14, 46, 51, 58]. Microscale modeling is based on more fundamental continuum mechanical principles than phenomenological macroscale approaches. Although the length scale of systems that can be modeled using microscale systems is continually increasing with evolving computational methods and computing hardware advances [57], a broad disparity exists between the length scale of feasible microscale simulations and applications of concern that require macroscale approaches [33]. This disparity of scales can be used as a basis for questioning the worth of microscale modeling beyond being an approach to advance fundamental understanding in some cases.

An alternative perspective is that macroscale models can be derived rigorously, maintaining a connection to fundamental microscale approaches, and closed in a thermodynamically consistent fashion. While various upscaling approaches exist that enable the development of such models, such as homogenization, volume averaging, and hybrid mixture theory [2, 29, 54], we focus our attention on the thermodynamically constrained averaging theory (TCAT) approach because this approach is applicable to a wide range of systems and is thermodynamically consistent across scales [19, 23, 25, 34]. Although TCAT methods have been used to formulate a broad range of models, the mathematical details of the approach pose a significant barrier to understanding and applying such models.

Our perspective is that models that are rigorously connected across scales are advantageous and that available results can be used to advance improved models and shed significant light on traditional approaches. We further assert that existing theoretical results can be used relatively easily to understand scale connections, thermodynamic constraints, why standard phenomenological approaches provide useful results in some cases, when phenomenological approaches are likely to be inadequate, and how to formulate rigorous new models by leveraging available results.

The goal of this work is to demonstrate how TCAT can be utilized for formulating, closing, and assessing macroscale models. The specific objectives of this work are: (1) to formulate essentially exact microscale and macroscale continuum models; (2) to illustrate how an exact macroscale model can be used to validate microscale numerical solutions and upscaling approximations; and (3) to show how extant entropy inequalities can be used to guide approximate model closure.

2 Model Formulation

2.1 Overview

TCAT provides an explicit connection across length scales [23]. This means that all macroscale equations and quantities can be expressed in an exact form based on some averaged form of microscale quantities. The purpose of this section is to formulate an essentially exact macroscale model—noting caveats that result from reliance on a microscale model that purists might not consider "exact" and the need to approximate averaging operators needed for

upscaling. This macroscale model will, in turn, be used to demonstrate the connection between scales, validate approximate microscale simulation and averaging methods, demonstrate the role of closure approximations, and illustrate the way in which an entropy inequality can be used to formulate closure relations needed to solve macroscale models. These elements will be achieved using an example of single-fluid flow through a porous medium system [20, 23].

TCAT model hierarchies are typically derived for general classes of models. A class of models is distinguished by the scale of the resultant model (e.g., macroscale, megascale (system scale), or some combination of scales); the entities present, including the phases, interfaces, common curves, and common points included in the model; the bulk or compositional nature of the transport phenomena of concern; and the underlying thermodynamic theory relied upon. This classification ensures that broad classes of models can be derived but that the formulated model complexity can be tractable. Once a formulated hierarchy is developed, it may be used for any model that is a subset of the hierarchy by applying a set of secondary restrictions [23]. The secondary restrictions specified here are: (1) an isothermal system, (2) a Newtonian fluid, (3) a solid phase that is immobile, incompressible, of a constant volume fraction and orientation in space and time, and having a constant mean and Gaussian curvature of the bounding surface at the microscale, (4) a massless interface of constant macroscale extent and interfacial tension, (5) an invariant composition of each phase, implying inter-entity mass exchange and reactions do not occur; (6) a nonlinear equation of state that relates the density and pressure of the fluid; and (7) the only body force is a constant gravitational acceleration vector. These restrictions are made to simplify and make more transparent the accomplishment of the objectives of the present work. The principles explored apply to more complicated and less restricted models derived from TCAT hierarchies as well. In the following sections, we use the enumerated restrictions to formulate an example that demonstrates and accomplishes the objectives of this presentation.

2.2 Microscale Model

Cornerstones of mechanistic continuum models are the principles of conservation of mass, momentum, and energy. Due to the isothermal nature of the restricted system considered, the conservation of mass and momentum equations are the equations of concern here. The system of concern was detailed through the secondary restrictions given in §2.1.

For a phase, the microscale conservation of mass equation can be written as [23, Eqn (2.21)]

$$\frac{\partial \rho_\alpha}{\partial t} + \nabla\cdot\left(\rho_\alpha \mathbf{v}_\alpha\right) = 0 \quad \text{for } \alpha \in \mathcal{I}_\mathrm{P}\ , \tag{1}$$

and the microscale conservation of momentum equation can be written as [23, Eqn (2.27)]

$$\frac{\partial (\rho_\alpha \mathbf{v}_\alpha)}{\partial t} + \nabla\cdot\left(\rho_\alpha \mathbf{v}_\alpha \mathbf{v}_\alpha\right) - \nabla\cdot\mathbf{t}_\alpha - \rho_\alpha \mathbf{g}_\alpha = 0 \quad \text{for } \alpha \in \mathcal{I}_\mathrm{P}\ , \tag{2}$$

where subscripts denote a microscale quantity, α is an entity qualifier, ρ is density, t is time, $\mathbf{v}$ is the velocity vector, $\mathbf{t}$ is the stress tensor, $\mathbf{g}$ is gravitational acceleration vector, $\mathcal{I}_\mathrm{P} = \{w, s\}$ is the index set of phases, w represents the fluid phase, and s represents the solid phase [23].

Because of the solid-phase restrictions, only the conservation equations of the fluid phase require solution, which would not be the case for a mobile, deformable solid phase. Eqns (1) and (2) are four scalar equations resulting in 10 unknowns, 1 from ρ_w, 3 from $\mathbf{v}_w$, and 6 from $\mathbf{t}_w$ due to symmetry, and assuming the body force is known. This deficit of six equations must be resolved for a solvable mechanistic model. The stress tensor for a Newtonian fluid is commonly expressed as

$$\mathbf{t}_w = -p_w \mathbf{I} + 2\hat{\mu}_w \mathbf{d}_w - \frac{2\hat{\mu}_w}{3}\left(\mathbf{I}\!:\!\mathbf{d}_w\right)\mathbf{I}\ , \tag{3}$$

where the rate of strain tensor is

$$\mathbf{d}_w = \frac{1}{2}\left[\nabla \mathbf{v}_w + (\nabla \mathbf{v}_w)^{\mathrm{T}}\right] , \tag{4}$$

p_w is the fluid pressure, $\hat{\mu}_w$ is the dynamic viscosity, $\mathbf{I}$ is the identity tensor, and the bulk viscosity has been neglected [7]. The sum of the last two terms in Eqn (3) comprise the viscous stress tensor, $\boldsymbol{\tau}_w$. Equation (3) provides relations for the six unknown components of the symmetric tensor $\mathbf{t}_w$, assuming $\hat{\mu}_w$ can be specified; but it also introduces the fluid pressure as a new variable that still leaves a deficit of one equation. This deficit can be resolved by specifying an equation of state of the form

$$\rho_w = f(p_w) , \tag{5}$$

where f can be specified based upon the isothermal, constant-composition conditions stated in the secondary restrictions given in §2.1. Eqns (3) and (5) are microscale equations that are well established for slightly compressible, Newtonian fluids—sufficiently so that they will be considered essentially exact for the purposes herein. Thus an essentially exact microscale model exists consisting of the microscale conservation of mass and momentum equations together with the Newtonian stress tensor and an equation of state. The goal then is to upscale and utilize this microscale model to illustrate the connection across scales, examine different flow regimes, validate numerical methods, and examine closure approximations constrained by the TCAT entropy inequality.

2.3 Macroscale Model

The conceptual approach and mathematical details of all parts of the TCAT approach are available in the literature and need not be repeated here [e.g., 19, 20, 23, 34, 36]. Instead, we will provide a brief summary and the relevant macroscale conservation equations consistent with the microscale model presented in §2.2. An exact form of these equations will be formulated to demonstrate the connection across scales and motivate the closure approach used in the TCAT model-building approach.

The TCAT approach produces macroscale equations by applying an averaging operator and averaging theorems to microscale equations. Both of these applications are exact; thus exact macroscale equations are derived based upon essentially exact microscale equations.

Applying an averaging operator and averaging theorems (Appendix A for definitions) to Eqn (1) yields the macroscale conservation of mass equation for the w phase given by [23, Eqn (6.60)]

$$\frac{\partial\left(\epsilon^{\overline{\overline{w}}}\rho^{w}\right)}{\partial t} + \nabla\cdot\left(\epsilon^{\overline{\overline{w}}}\rho^{w}\mathbf{v}^{\overline{w}}\right) = 0 , \tag{6}$$

where superscripts denote a macroscale quantity, $\epsilon^{\overline{\overline{w}}}$ is a volume fraction, ρ^w is an average density, t is time, and $\mathbf{v}^{\overline{w}}$ is a density-weighted velocity. Eqn (6) does not include a mass exchange term because of the secondary restrictions applied to the system of focus. The precise definitions of all averaged quantities ensure a connection between the microscale and the macroscale for all quantities appearing in these equations.

For an averaging domain Ω of fixed volume regardless of location within the system, an exact constraint equation follows in light of the restrictions on the solid phase such that

$$\epsilon^{\overline{\overline{w}}} = \epsilon , \tag{7}$$

where ϵ is a specified constant porosity for the system.

Macroscale conservation of momentum equations can be derived in a similar fashion by averaging and simplifying Eqn (2) yielding the macroscale equation given by [23, Eqn (6.92)]

$$\frac{\partial\left(\epsilon^{\overline{\overline{w}}}\rho^{w}\mathbf{v}^{\overline{w}}\right)}{\partial t}+\nabla\cdot\left(\epsilon^{\overline{\overline{w}}}\rho^{w}\mathbf{v}^{\overline{w}}\mathbf{v}^{\overline{w}}\right)-\nabla\cdot\left(\epsilon^{\overline{\overline{w}}}\mathbf{t}^{\overline{\overline{w}}}\right)-\epsilon^{\overline{\overline{w}}}\rho^{w}\mathbf{g}^{\overline{w}}-\overset{s\to w}{\mathbf{T}}=0\,, \tag{8}$$

where $\mathbf{t}^{\overline{\overline{w}}}$ is the macroscale stress tensor, $\mathbf{g}^{\overline{w}}$ is a density-weighted averaged body force vector, $\overset{s\to w}{\mathbf{T}}$ represents momentum exchange from the solid phase to the fluid phase. Momentum exchange resulting from mass exchange between entities is omitted from Eqn (8) because of the specified restriction precluding mass exchange. Specific forms of $\mathbf{t}^{\overline{\overline{w}}}$ and $\overset{s\to w}{\mathbf{T}}$ that link the microscale and the macroscale are available, supporting the essentially exact nature of Eqn (8).

Averaging from the microscale to the macroscale results in the definition of the macroscale stress tensor given by [23, Eqn (6.92)]

$$\mathbf{t}^{\overline{\overline{w}}}=\left\langle\mathbf{t}_{w}-\rho_{w}\left(\mathbf{v}_{w}-\mathbf{v}^{\overline{w}}\right)\left(\mathbf{v}_{w}-\mathbf{v}^{\overline{w}}\right)\right\rangle_{\Omega_{w},\Omega_{w}}\,, \tag{9}$$

where the brackets denote an averaging operator (Appendix A) and the subscripts denote the region of integration and the normalization region, respectively, both of which are the domain of the w fluid phase within the averaging region denoted by Ω_w. A complete derivation of this expression and details on various forms of the averaging operator are available in the literature [23, 34]. To evaluate the macroscale stress tensor from Eqn (9), microscale information is needed for $\mathbf{v}_w$ and for the stress tensor denoted $\mathbf{t}_w$, given in Eqn (3).

Averaging from the microscale to the macroscale yields the definition of the inter-entity transfer of momentum given by [23, Eqn (6.85)]

$$\overset{s\to w}{\mathbf{T}}=\left\langle\mathbf{t}_{w}\cdot\mathbf{n}_{w}\right\rangle_{\Omega_{ws},\Omega}\,, \tag{10}$$

where $\mathbf{n}_w$ is the unit normal vector pointing outward from the w phase at the interface between the w and s phases, and integration is over this interface, Ω_{ws}. Normalization is over the averaging region domain, Ω.

Eqns (6) and (8) specify a macroscale model for the single-phase flow problem considered here. Since ρ^w is an intrinsic average, it can be computed by applying an averaging operator to Eqn (5)

$$\rho^{w}=\left\langle\rho_{w}\right\rangle_{\Omega_{w},\Omega_{w}}=\left\langle f(p_{w})\right\rangle_{\Omega_{w},\Omega_{w}}\neq f(p^{w})\,, \tag{11}$$

resulting in a system of five equations in five unknowns that is solvable if a microscale solution exists. For nonlinear equations of state—assumed here, the form of Eqn (5) cannot be assumed to apply directly at the macroscale, which is noted in this equation.

Thus we have an essentially exact macroscale model for this specific case, provided we have a microscale solution to Eqns (9), (10), and (11). When a microscale solution is unavailable, which is generally the case, alternative closure relations are needed (see §4). Note that some error will occur in approximating the averaging operators needed to produce the macroscale solution from the microscale solution. This demonstrates that a firm connection across scales exists. This connection can be used as a microscale simulation validation. Any accurate microscale numerical solution and averaging upscaling procedure must satisfy the derived macroscale model. The extent to which this macroscale model is not satisfied is a measure of numerical approximation error. Even for the case in which only a microscale solution is desired, real-time computation of the macroscale model solution provides a valuable means to monitor the reliability of the microscale solution.

2.4 Thermodynamic Considerations

A distinct and unique feature of TCAT is that it averages thermodynamic relations from the microscale to the macroscale. This is done to maintain a clear connection between thermodynamic relations and variables well-understood at the microscale to relations and quantities at the macroscale. In some approaches to obtaining larger scale equations, thermodynamics at the microscale is not part of the analysis (e.g., in the fine work that led to Darcy's law of flow [12, 13] and the postulation of Fourier's law of heat conduction [17, 44]). In other approaches, microscale thermodynamics is bypassed with thermodynamic relations being proposed directly at the larger scale (e.g., in early averaging efforts for porous media [28] and persisting in the porous media literature and its offshoots to the present [6, 59]). When proposed at the larger scale, the relations employed are typically referred to as part of a thermodynamically "consistent" model [e.g., 42, 45]. These "consistent" models indeed have the trappings of thermodynamics with thermodynamic relations that appear to mimic those at the microscale. Unfortunately, the quantities are not tied to microscale precursors and thus are undefined and unmeasurable. For example, indicating a quantity to be p^α does not necessarily mean that it is pressure or that it is rooted in a well-defined microscale pressure. Furthermore, these "consistent" approaches typically make use of rational thermodynamics, an approach that is not without controversy [32, 43, 49, 50, 55, 56], and which has the feature that temperature is considered to be a primitive variable that actually has no correspondence with temperature as employed in classical irreversible thermodynamics. The challenges associated with averaging also confound the use of rational thermodynamics to provide consistent, testable models.

Müller has commented, "If the truth were known and admitted, rational thermodynamics is not all that different from the thermodynamics of irreversible processes" [43], the latter being the formulation that we employ. He has also noted that it is now accepted by most people that rational thermodynamics cannot be used for non-linear problems. These comments suggest that the use of rational thermodynamics, as it often is as an essential aspect of what is called hybrid mixture theory, is inappropriate. The absence of any relation between large-scale and small-scale properties is the primary shortcoming.

We observe that thermodynamics in its purest form is posited for equilibrium systems with no spatial gradients. When this situation applies, the equivalence among properties at any scale above the microscale is assured. The extension of thermodynamics to systems away from equilibrium is the cause of complications. The local equilibrium assumption applies the restriction that relations among thermodynamic variables that apply for an equilibrium system apply locally, i.e., at a microscale point. Thus, variables need not be uniform but may vary in space from point to point. It is this variability that creates the challenges in defining larger-scale, averaged variables.

Extensive quantities may be integrated over their associated regions. Mass per volume, momentum per volume, and energy per volume may be integrated over a volume to obtain their extensive counterparts. There is no ambiguity. Division of the extensive mass by the integration volume gives the average mass density. Division of the extensive momentum by the extensive mass gives the average velocity. There is no similar unambiguous approach to defining intensive variables. For example, average temperature could be defined as an average over a volume, as an average weighted by heat capacity, as an average weighted by entropy, or by any averaging procedure that one chooses to define. Because of this challenge, it is not sufficient to identify a macroscopic intensive quantity without also explicitly noting the procedure used to derive that macroscale quantity from a microscale precursor.

As an example of the importance of defining macroscale temperature, the Euler equation for a pure fluid has been obtained by averaging to obtain [23, Eqn (7.13)]

$$E^\alpha = \theta^{\overline{\overline{\alpha}}}\eta^\alpha - p^\alpha + \rho^\alpha \mu^{\overline{\alpha}} \,, \tag{12}$$

where E is internal energy per volume, η is entropy per volume, θ is temperature, p is pressure, ρ is mass density, and μ is chemical potential. In this equation, quantities with a superscript α have been obtained by averaging their microscale counterparts over a volume; chemical potential has superscript $\overline{\alpha}$ to indicate that it has been obtained as a mass density weighted average of microscale chemical potential. We have used the superscript $\overline{\overline{\alpha}}$ to indicate that the average employed is some particular version that must be defined. For temperature, we use the entropy weighted average such that [23, Eqn (7.5)]

$$\theta^{\overline{\overline{\alpha}}} = \frac{\int\limits_{\Omega_\alpha} \eta_\alpha \theta_\alpha \, \mathrm{d}\mathfrak{r}}{\int\limits_{\Omega_\alpha} \eta_\alpha \, \mathrm{d}\mathfrak{r}} \, . \tag{13}$$

The implications of this feature can be noticed, for example, if we average the ideal gas equation

$$p_\alpha = \rho_\alpha \hat{R} \theta_\alpha \, , \tag{14}$$

where $\hat{R}$ is a constant equal to the ideal gas constant divided by the molecular weight of the gas in the α phase. Averaging of this equation by integrating over a volume gives

$$p^\alpha = \rho^\alpha \hat{R} \theta^{\overline{\alpha}} \, . \tag{15}$$

Therefore, we have two different indexes of macroscale temperature. They will be equal only if the entropy-weighted average temperature is equal to the mass-density-weighted average temperature. When they are not equal, either the Euler form of Eqn (12) or the equation of state in Eqn (15) will have to be modified if only a single macroscopic temperature measure is to be used in an analysis. This result shows that an equation of state or a constitutive relation appropriate for one scale does not necessarily transfer directly to a larger scale. This observation is important for obtaining definitions of other intensive variables, such as pressure and chemical potential, which could be averaged to obtain large scale values using different weighting coefficients or domains of averaging. Using the TCAT approach, we are careful to ensure that macroscale variables are uniquely and explicitly defined in terms of the averaging procedure used to transition to the macroscale.

3 Computational Approach

3.1 Overview

To illustrate how scale consistency can be used to validate microscale numerical solutions and inform macroscale closure approximations, the microscale governing equations were solved numerically for three porous medium domains. From the microscale solutions, macroscale variables were calculated, where the macroscale domain was defined as the entire microscale domain, and thus can be represented as a single point. The microscale simulation approach, the domains analyzed, as well as the methods used to calculate macroscale variables from the microscale solution are presented.

3.2 Finite Volume Methods

The open-source, computational fluid dynamics package OpenFOAM (v2406) was used for all microscale simulations [53]. To allow for tailored numerical approximations, the following

form of microscale governing equations were solved

$$\frac{\partial \rho_w}{\partial t} + \nabla \cdot (\rho_w \mathbf{v}_w) = 0 \ , \tag{16}$$

and

$$\frac{\partial (\rho_w \mathbf{v}_w)}{\partial t} + \nabla \cdot (\rho_w \mathbf{v}_w \mathbf{v}_w) - \nabla \cdot \boldsymbol{\tau}_w + \nabla p'_w + \mathbf{g}_w \cdot \mathbf{h} \nabla \rho_w = 0 \ , \tag{17}$$

where $p'_w = p_w - \rho_w \mathbf{g}_w \cdot \mathbf{h}$, $\mathbf{h}$ is a position vector, and gravity is assumed constant. A steady-state solver was implemented, where the `simple` algorithm was used to solve the governing equations [51]. This algorithm performs iterative under-relaxation until a specified error tolerance is met. In this work, the magnitude of Eqn (8) was the error measure and a maximum allowable tolerance of 10^{-8} was specified. Linear solver tolerances were set such that the residual of Eqn (8) was the leading source of error.

3.3 Porous Medium Domains

Three periodic porous medium domains were generated for this work. A sphere-packing code was used to generate 50 uniform (radii = 1 mm) and 50 log-normally distributed (mean = 0.1 mm, standard deviation = 0.5 mm) spheres for two of the domains [1]. For the third domain, an additional set of 50 uniform spheres (radii = 1 mm) were packed in a non-cubic domain and then converted to ellipsoids by shrinking the domain in a direction orthogonal to the primary direction of flow by a factor of 2.0 [9]. Table 1 contains geometric measures for each domain including the specific surface area of the ws interface ($\epsilon^{\overline{\overline{ws}}}$) and Figure 1 depicts the domains.

Table 1: Geometric Measures of the Porous Media Domains

Property	Uniform	Log-normal	Ellipsoid
Simulated Volume (mm^3)	6.69^3	10.5^3	5.94^3
$\epsilon^{\overline{\overline{w}}}$ (unitless)	0.394	0.346	0.454
$\epsilon^{\overline{\overline{ws}}}$ (mm^{-1})	1.81	1.01	2.05
Sauter Mean Diameter (mm)	9.25	11.4	7.21

To generate computational meshes, a background mesh of 200^3 was used along with `snappyHexMesh`, a mesh generation tool accompanied with OpenFOAM, to resolve the solid phase. Similar to the work in [9], near surface refinement of level 2 was used to accurately model the surface of the solid, however, snapping was also used to further improve the mesh quality and resolution of the ws interface. The resultant meshes had an average of 3.5×10^7 (330^3) cells.

3.4 Simulation Specifics

For the simulations, water was assumed to be the fluid. As such, the viscosity ($\hat{\mu}_w$) was set to 8.9×10^{-4} g/mm-s and the density was defined as

$$\rho_w = \rho_{w,0} e^{\hat{\beta} p_w} \ , \tag{18}$$

where $\rho_{w,0} = 10^{-3}$ g/mm^3, and $\hat{\beta} = 10^{-10}$ mm-s^2/g. Cyclic boundary conditions were applied on all boundaries except the inlet and outlet boundaries. The velocity at the inlet

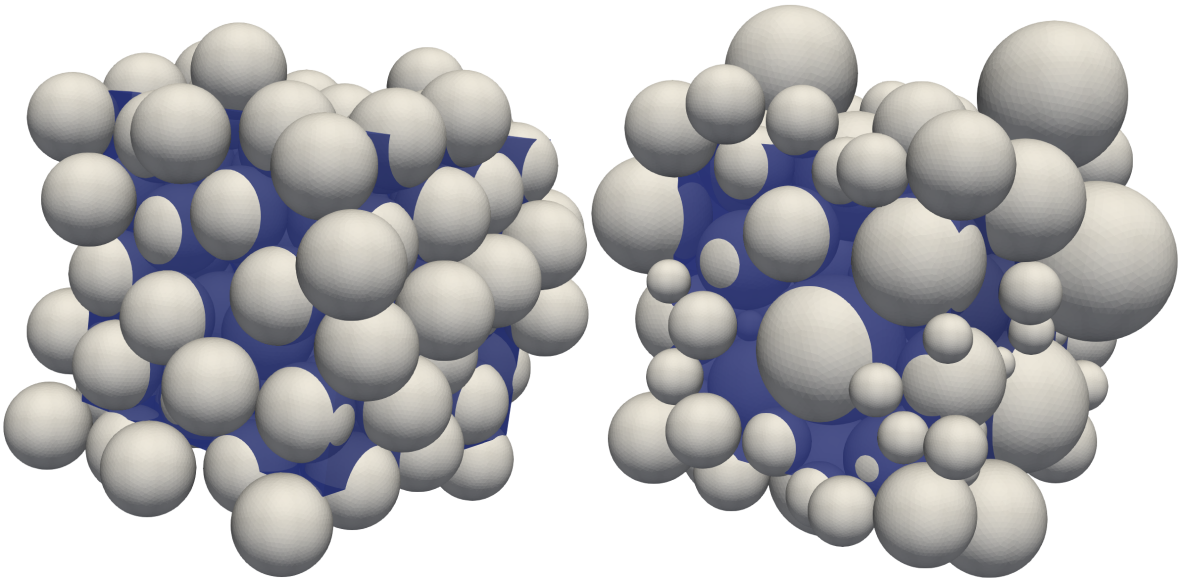

(a) Uniform

(b) Log-normal

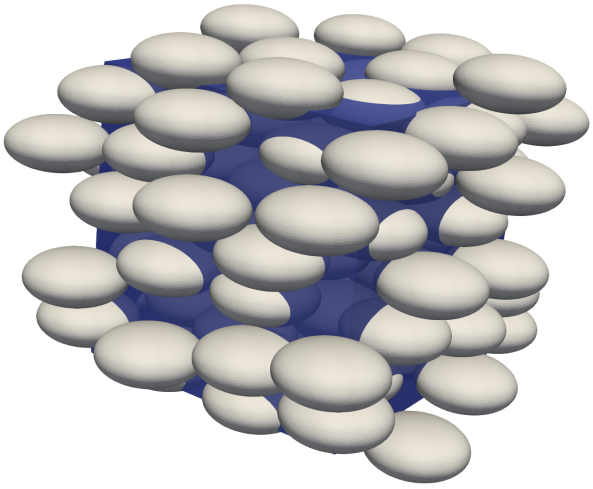

(c) Ellipsoid

Figure 1: Porous medium domains examined where the computational meshes consisted of the portions shown in blue.

was calculated from a specified macroscale mass flow rate (m_{in}) entering the system given as

$$\int_{\Gamma_{\text{in}}} \rho_w \mathbf{v}_w \cdot \mathbf{n}_w \, \mathrm{d}\mathfrak{r} = m_{\text{in}} \, , \tag{19}$$

and a zero gradient boundary condition was applied at the outlet

$$\left(\nabla \mathbf{v}_w \cdot \mathbf{n}_w\right) |_{\text{out}} = \mathbf{0} \, . \tag{20}$$

A no-slip condition was used on the ws interface, defined as

$$\left(\mathbf{v}_w \cdot \mathbf{n}_w\right) |_{\Omega_{ws}} = \mathbf{0} \, . \tag{21}$$

The inlet mass flow rates ranged from 1×10^{-7} – 3.0×10^{-1} g/s resulting in 32 simulations per domain. The other solution variable, p'_w, was calculated based on the specified velocity at the inlet and set to a value of 0 g/mm-s^2 at the outlet. On the ws interface, a zero gradient condition was applied, given as,

$$\left(\nabla p'_w \cdot \mathbf{n}_w\right) |_{\Omega_{ws}} = \mathbf{0} \, . \tag{22}$$

$|\mathbf{g}_w|$ was set to 9.81×10^3 mm/s^2 for all simulations. Only state-state simulations were considered so no initial conditions were required.

3.5 Macroscale Verification of Microscale Simulations

Macroscale quantities were calculated from microscale simulation results for the domains presented based on their formal definitions and through use of the transport theorems (Appendix A) [24]. We treat the microscale domain as a single macroscale averaging region. To ensure the accurate construction of macroscale quantities, the same numerical approaches that were used to solve the governing equations were used to determine the macroscale variables. Failure to do so can result in significant errors in the macroscale variables. For example, in OpenFOAM, pressure is decomposed as shown in §3.2, and the macroscale pressure gradient was calculated with the averaging operator and gradient theorem as

$$\nabla p^w = \langle \nabla p_w \rangle_{\Omega_w,\Omega} + \langle p_w \mathbf{n}_w \rangle_{\Omega_{ws},\Omega} \, , \tag{23}$$

where $\nabla p_w = \nabla p'_w + \rho_w \mathbf{g}_w + \mathbf{g}_w \cdot \mathbf{h} \nabla \rho_w$, resulting in

$$\nabla p^w = \left\langle \nabla p'_w + \rho_w \mathbf{g}_w + \mathbf{g}_w \cdot \mathbf{h} \nabla \rho_w \right\rangle_{\Omega_w,\Omega} + \left\langle \left(p'_w + \rho_w \mathbf{g}_w \cdot \mathbf{h}\right) \mathbf{n}_w \right\rangle_{\Omega_{ws},\Omega} \, . \tag{24}$$

Note that the average of a microscale derivative is not, in general, the derivative of a macroscale average and a boundary term arises that must be included. The term $\nabla p'_w$ is computed at cell faces of the computational mesh as opposed to other gradients that are determined at cell centers. Due to the mass density weighting that is often used for defining macroscale variables with TCAT [23], it is convenient to determine macroscale derivative terms thorough application of the product rule. To demonstrate this, the gradient of macroscale chemical potential ($\mu^{\overline{w}}$) is computed as

$$\begin{aligned} \epsilon^{\overline{\overline{w}}} \rho^w \nabla \mu^{\overline{w}} = & \langle \rho_w \nabla \mu_w + \mu_w \nabla \rho_w \rangle_{\Omega_w,\Omega} - \langle \rho_w \mu_w \mathbf{n}_w \rangle_{\Omega_{ws},\Omega} \\ & - \langle \mu_w \rangle_{\Omega_w,\Omega_w,\rho_w} \left[\langle \nabla \rho_w \rangle_{\Omega_w,\Omega} - \langle \rho_w \mathbf{n}_w \rangle_{\Omega_{ws},\Omega} \right] \, , \end{aligned} \tag{25}$$

where

$$\mu_w = \frac{1}{\rho_{w,0} \hat{\beta}} \left(1 - e^{-\hat{\beta} p_w}\right) \, . \tag{26}$$

Further, we make use of the Gibbs-Duhem relation [23, Eqn (3.43)], $\rho_w \nabla \mu_w = \nabla p_w$ and Eqn (24) to calculate the macroscale gradient from the solution variables. The gradient of the macroscale gravitational potential ($\psi^{\overline{w}}$) is calculated from microscale precursors as

$$\begin{aligned} \epsilon^{\overline{\overline{w}}} \rho^{w} \nabla \psi^{\overline{w}} = & \langle -\rho_w \mathbf{g}_w + \psi_w \nabla \rho_w \rangle_{\Omega_w,\Omega} - \langle \rho_w \psi_w \mathbf{n}_w \rangle_{\Omega_{ws},\Omega} \\ & - \langle \psi_w \rangle_{\Omega_w,\Omega_w,\rho_w} \left[\langle \nabla \rho_w \rangle_{\Omega_w,\Omega} - \langle \rho_w \mathbf{n}_w \rangle_{\Omega_{ws},\Omega} \right] , \end{aligned} \tag{27}$$

where $\nabla \psi_w = -\mathbf{g}_w$ [23, Eqn (2.50)].

Parallelization in OpenFOAM is accomplished through domain decomposition [53]. For each subdomain, the full suite of macroscale variables were computed. All macroscale data, however, is shown for a single averaging region that contains the entire computational domain (i.e. the macroscale integrals were summed across subdomains and then normalized).

Figure 2 shows the magnitude of the residual for the macroscale conservation of mass and momentum equations [Eqns (6) and (8)] where all terms were determined from averaging microscale simulation results. Convergence was declared once the magnitude of Eqn (8) was less than the allowable tolerance. No restrictions were placed on the macroscale conservation of mass equation, and we see the magnitude of the residual increase as the Reynolds number (Re) increases. This validation process not only ensures the numerical accuracy of the microscale simulations, but also our ability to accurately compute macroscale variables, and consistency with the exact form of the macroscale model.

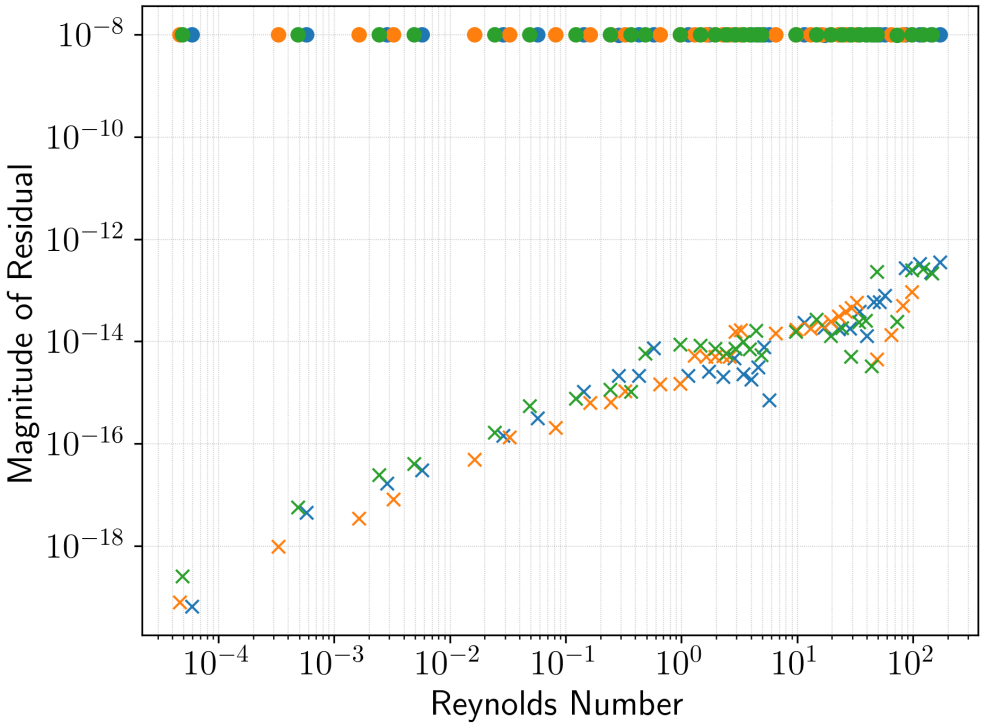

Figure 2: The magnitude of the residual for Eqn (6) and Eqn (8) shown with crosses and circles, respectively, for the uniform (blue), log-normal (orange), and ellipsoid (green) domains.

4 Macroscale Model Closure

4.1 Overview

The exact model formulated in §2.3 is closed only because it was assumed that a microscale solution existed. Specifically, $\mathbf{t}^{\overline{\overline{w}}}$ was defined with Eqn (9), $\overset{s\to w}{\mathbf{T}}$ was defined with Eqn (10), and ρ^w was defined with Eqn (11), all of which are expressions involving microscale quantities. Lacking such a microscale solution, approximations of these three quantities are needed as a function of other macroscale quantities that are resolved. The connection between the microscale and macroscale models can be used to inform the approximate closure, parameterization, and evaluation processes for the macroscale model.

The closure of macroscale models is often approached phenomenologically based upon observational support [5]. While this approach has resulted in useful solutions in some cases, a more rigorous, theoretical approach is more illuminating and generally applicable [9, 22, 52]. The TCAT approach provides a framework for formulating and closing models, which can be applied to the macroscale example considered herein [20]. Consideration of the formulation and closure of this single-fluid macroscale model is sufficient to demonstrate the advantages of the TCAT approach and the manner in which available results can be used. In the sections that follow, the role of the entropy inequality, and macroscale closure for Stokes and transition flow are presented.

4.2 TCAT Entropy Inequality

The TCAT approach provides the connection between scales of conservation equations, thermodynamic principles, and kinematic evolution equations based upon averaging theorems [23, 26]. While the TCAT macroscale equations provide the connection between the microscale and the macroscale, as previously shown, these equations alone in the absence of a microscale solution do not provide closed macroscale models. Because of this observation, an important component of TCAT is the entropy inequality, which is useful for generating the closure relations needed to formulate closed macroscale models. The entropy inequality relates the sum of the products of fluxes and forces to the entropy production rate, which must be a non-negative quantity for consistency with the second law of thermodynamics [23]. The flux and force formulation is routinely used in irreversible thermodynamics [7]. While these entropy inequality expressions can be long and off-putting, spanning multiple pages in some instances, they are highly useful. The usefulness of these expressions arises from reasoning that can be performed to ensure that closure relations that are posited are consistent with the entropy inequality and known equilibrium conditions. Alternatively stated, the entropy inequality provides a set of permissibility conditions constraining valid closure approximations. Ignoring the entropy inequality in generating closure approximations, for example by proceeding based upon phenomenological approaches alone, runs the risk of producing relations that violate the second law of thermodynamics and thus cannot be correct [38, 40].

Being more explicit, a macroscale balance of entropy equation has been developed of the form [23, Eqn (9.1)]

$$\mathcal{S}_*^{\overline{\overline{\alpha}}} = \Lambda^{\overline{\overline{\alpha}}} \quad \text{for } \alpha \in \mathcal{I}\,, \tag{28}$$

where $\mathcal{S}_*^{\overline{\overline{\alpha}}}$ is defined as the sum of the accumulation, advective transport, non-advective transport, inter-entity exchange, and source of entropy; $\Lambda^{\overline{\overline{\alpha}}}$ is the entropy production rate density; and $\mathcal{I}$ is the set of all entities for $\mathcal{I} = \{w, s, ws\}$ for the case of single-fluid flow with ws being the interface between the phases. While detailed representations of each component of $\mathcal{S}_*^{\overline{\overline{\alpha}}}$ are available and resemble the conservation equations, a shorthand form is adequate for the

purpose at hand. The second law of thermodynamics requires that [23, Eqn (9.5)]

$$\sum_{\alpha\in\mathcal{I}} \mathcal{S}_*^{\overline{\overline{\alpha}}} = \sum_{\alpha\in\mathcal{I}} \Lambda^{\overline{\overline{\alpha}}} = \Lambda \geq 0 \,, \tag{29}$$

where Λ is the total entropy production rate density for the system.

While Eqn (29) is a precise statement of the second law of thermodynamics, it is not of a form that is of optimal use for constraining the form of closure relations for mechanistic models. A more useful form transforms the left-hand-side of Eqn (29) into a sum of the products of fluxes and forces representing dissipative processes that are known to potentially generate entropy. To arrive at this more useful form, it is necessary to connect the conservation equations, which include the dissipative processes of interest, to the entropy balance equation, which is accomplished using thermodynamic equations. While any thermodynamic theory can be selected within the TCAT approach, classical irreversible thermodynamics has been relied upon for the results relevant here [20, 23].

The connection between dissipative processes and the entropy production rate can be derived by formulating an alternative statement of the second law of thermodynamics, which can be written as the augmented entropy inequality given by [23, Eqn (9.20)]

$$\begin{aligned}\sum_{\alpha\in\mathcal{I}} \mathcal{S}_*^{\overline{\overline{\alpha}}} + \sum_{\alpha\in\mathcal{I}} \lambda_{\mathcal{E}}^{\alpha}\mathcal{E}_*^{\overline{\overline{\alpha}}} + \sum_{\alpha\in\mathcal{I}} \boldsymbol{\lambda}_{\boldsymbol{\mathcal{P}}}^{\alpha}\boldsymbol{\cdot}\boldsymbol{\mathcal{P}}_*^{\overline{\overline{\alpha}}} + \sum_{\alpha\in\mathcal{I}} \lambda_{\mathcal{M}}^{\alpha}\mathcal{M}_*^{\overline{\overline{\alpha}}} + \sum_{\alpha\in\mathcal{I}} \lambda_{\mathcal{G}}^{\alpha}\mathcal{G}_*^{\overline{\overline{\alpha}}} + \sum_{\alpha\in\mathcal{I}} \lambda_{\mathcal{T}}^{\alpha}\mathcal{T}_*^{\overline{\overline{\alpha}}} + \sum_{\alpha\in\mathcal{I}} \lambda_{\mathcal{T}\mathcal{G}}^{\alpha}\mathcal{T}_{\mathcal{G}*}^{\overline{\overline{\alpha}}} \\ = \sum_{\alpha\in\mathcal{I}} \Lambda^{\overline{\overline{\alpha}}} = \Lambda \geq 0 \,,\end{aligned} \tag{30}$$

where all adorned λ are Lagrange multipliers that form a product with a respective conservation or thermodynamic equation, $\mathcal{E}_*^{\overline{\overline{\alpha}}}$ represents conservation of energy equations, $\boldsymbol{\mathcal{P}}_*^{\overline{\overline{\alpha}}}$ represents conservation of momentum equations, $\mathcal{M}_*^{\overline{\overline{\alpha}}}$ represents conservation of mass equations, $\mathcal{G}_*^{\overline{\overline{\alpha}}}$ represents potential energy equations, $\mathcal{T}_*^{\overline{\overline{\alpha}}}$ represents thermodynamic equations, and $\mathcal{T}_{\mathcal{G}*}^{\overline{\overline{\alpha}}}$ represents derivatives of potential energy equations. The complete details of each of these equations have been derived and are available in the literature but are not necessary for the present discussion [23]. As an example, $\mathcal{M}_*^{\overline{\overline{w}}}$ is a material derivative form of Eqn (6) and $\boldsymbol{\mathcal{P}}_*^{\overline{\overline{w}}}$ is a material derivative form of Eqn (8). Just as with these examples, all equations multiplied by Lagrange multipliers are arranged in a form such that they are equal to zero—preserving the validity of the statement of the entropy production rate while providing a means to introduce dissipative processes into the formulation.

Because each of the placeholder variables represents an entire equation, it can be observed that a fully expanded version of Eqn (30) is a lengthy expression that on the surface does not convey much meaning. The details of this form are not needed here. What is useful to note is that a desired form of this equation can be written as

$$\sum_{i\in\mathcal{V}_s} J_i F_i + \sum_{i\in\mathcal{V}_v} \mathbf{J}_i\boldsymbol{\cdot}\mathbf{F}_i + \sum_{i\in\mathcal{V}_t} \mathbf{J}_i\boldsymbol{:}\mathbf{F}_i = \Lambda \geq 0 \,, \tag{31}$$

where the J terms represent fluxes, the F terms represent forces; the first grouping is a scalar pairing, the second grouping a vector pairing, and the third grouping a tensor pairing of fluxes and forces; $\mathcal{V}_s$ is the set of scalar quantities; $\mathcal{V}_v$ is the set of vector quantities;, and $\mathcal{V}_t$ is the set of tensor quantities. Substantial manipulations are needed to arrive at Eqn (31), and once-completed these manipulations do not need to be repeated for formulation of closure relations for a new model from the same basic class of models [20, 23]. Thus, available results can be reused, allowing rigorous derivations to be performed relatively quickly and efficiently.

Some additional details can shed some light on the manipulations needed to arrive at equations of the form of Eqn (31). The Lagrange multipliers in Eqn (30) are free parameters

since they multiply equations that are zero. These parameters are selected to eliminate material derivatives that are known to vanish at equilibrium, and the solution to meet this goal also conveys the convenient property of assuring that the resultant equation is dimensionally consistent [23, Eqns (9.25)–(9.30)]. Collecting of related terms from various equations and simplifying to a form informed by known equilibrium conditions produces a constrained entropy inequality, which while exact and of archival value is not in pure flux-force form. A pure flux-force form, as is shown abstractly in Eqn (31), requires approximations and is referred to as a simplified entropy inequality (SEI). To be fair, this can be considered somewhat of a misnomer for a general model hierarchy as the expressions may not appear simple to many.

Model hierarchies in TCAT are usually chosen with sufficient generality so as to support a range of models, leveraging general results for multiple uses. Subsets of a general model hierarchy can be specified after a general SEI has been developed, which enables simplifications of the general form. For example, an available SEI restricted to the case of isothermal conditions with no mass exchange can be written as [23, Eqn (9.63)]

$$
\begin{aligned}
&\frac{1}{\theta}\left(\epsilon^{\overline{\overline{w}}}\mathbf{t}^{\overline{\overline{w}}}+\epsilon^{\overline{\overline{w}}}p^{w}\mathbf{I}\right):\mathbf{d}^{\overline{\overline{w}}}+\frac{1}{\theta}\left(\epsilon^{\overline{\overline{s}}}\mathbf{t}^{\overline{\overline{s}}}-\epsilon^{\overline{\overline{s}}}\mathbf{t}^{s}\right):\mathbf{d}^{\overline{\overline{s}}}\\
&+\frac{1}{\theta}\left[\epsilon^{\overline{\overline{ws}}}\mathbf{t}^{\overline{\overline{ws}}}-\epsilon^{\overline{\overline{ws}}}\gamma^{ws}\left(\mathbf{I}-\mathbf{G}^{ws}\right)\right]:\mathbf{d}^{\overline{\overline{ws}}}\\
&+\frac{1}{\theta}\left[\nabla\left(\epsilon^{\overline{\overline{w}}}p^{w}\right)-\epsilon^{\overline{\overline{w}}}\rho^{w}\nabla\left(\mu^{\overline{w}}+\psi^{\overline{w}}\right)-\epsilon^{\overline{\overline{w}}}\rho^{w}\mathbf{g}^{\overline{w}}+\overset{w\to ws}{\mathbf{T}}\right]\cdot\left(\mathbf{v}^{\overline{w}}-\mathbf{v}^{\overline{s}}\right)\\
&-\frac{1}{\theta}\left\{\nabla\cdot\left[\left(\mathbf{I}-\mathbf{G}^{ws}\right)\epsilon^{\overline{\overline{ws}}}\gamma^{ws}\right]+\overset{w\to ws}{\mathbf{T}}+\overset{s\to ws}{\mathbf{T}}\right\}\cdot\left(\mathbf{v}^{\overline{ws}}-\mathbf{v}^{\overline{s}}\right)\\
&-\frac{1}{\theta}\frac{\mathrm{D}^{\overline{s}}\epsilon^{\overline{\overline{s}}}}{\mathrm{D}t}\left[p_{w}^{ws}+\langle\mathbf{n}_{s}\cdot\mathbf{t}_{s}\cdot\mathbf{n}_{s}\rangle_{\Omega_{ws},\Omega_{ws}}+\gamma^{ws}J_{s}^{ws}\right]=\sum_{\alpha\in\mathcal{J}}\Lambda^{\overline{\overline{\alpha}}}\geq 0\,,
\end{aligned}
\tag{32}
$$

where $\mathbf{d}^{\overline{\overline{\alpha}}}=[\nabla\mathbf{v}^{\overline{\alpha}}+(\nabla\mathbf{v}^{\overline{\alpha}})^{\mathrm{T}}]/2$ is the macroscale deformation rate tensor for the α entity, γ^{ws} is the interfacial tension of the ws interface, $\mathbf{G}^{ws}$ is a geometric orientation tensor for the ws interface, p_{w}^{ws} is the pressure of water phase averaged over the ws interface, and J_{s}^{ws} is twice the mean curvature of the ws interface. This SEI can be simplified further because of the additional restrictions specified for the class of problem being considered. Because the solid phase and interfaces are motionless and of a constant extent, interfacial tension, and orientation, Eqn (32) can be written as

$$
\begin{aligned}
&\frac{1}{\theta}\left(\epsilon^{\overline{\overline{w}}}\mathbf{t}^{\overline{\overline{w}}}+\epsilon^{\overline{\overline{w}}}p^{w}\mathbf{I}\right):\mathbf{d}^{\overline{\overline{w}}}\\
&+\frac{1}{\theta}\left[\nabla\left(\epsilon^{\overline{\overline{w}}}p^{w}\right)-\epsilon^{\overline{\overline{w}}}\rho^{w}\nabla\left(\mu^{\overline{w}}+\psi^{\overline{w}}\right)-\epsilon^{\overline{\overline{w}}}\rho^{w}\mathbf{g}^{\overline{w}}-\overset{s\to w}{\mathbf{T}}\right]\cdot\mathbf{v}^{\overline{w}}=\Lambda\geq 0\,,
\end{aligned}
\tag{33}
$$

where only two flux-force pairs remain for this example. This SEI can be used to generate closure relations for macroscale models, which are not unique but must be consistent with Eqn (33) and provides a connection between variables that arise from conservation equations (e.g., $p^{w},\mathbf{d}^{\overline{\overline{w}}}$) and thermodynamic variables (e.g., $\mu^{\overline{w}},\psi^{\overline{w}}$).

4.3 Stokes Flow

Macroscale models of general use are approximate because the microscale quantities relied upon above to formulate an exact model are not available unless a microscale solution already

exists. Thus, an approximate macroscale model is sought. Consider the case of Stokes flow at the microscale for which Eqn (2) simplifies to the form [7, Eqn (3.5-8)]

$$\nabla\cdot\mathbf{t}_w + \rho_w\mathbf{g}_w = 0\ . \tag{34}$$

Note that the accumulation and nonlinear advective transport of momentum terms vanish in the Stokes limit that corresponds to $\mathrm{Re} \ll 1$, where

$$\mathrm{Re} = \frac{\rho_w\mathbf{v}_w\ell}{\hat{\mu}_w}\ , \tag{35}$$

and ℓ is a characteristic length scale that can be taken as the Sauter mean particle diameter for a porous medium system. Eqn (34) is a linear momentum equation, which can be averaged to the macroscale giving

$$\nabla\cdot\left(\epsilon^{\overline{\overline{w}}}\mathbf{t}^w\right) + \epsilon^{\overline{\overline{w}}}\rho^w\mathbf{g}^{\overline{w}} + \overset{s\to w}{\mathbf{T}} = 0\ , \tag{36}$$

where $\mathbf{t}^w$ is an intrinsic average of the microscale stress tensor and not the macroscale form given by Eqn (9). The difference in form results from imposing the Stokes flow limit at the microscale in deriving Eqn (36). While simpler in form than Eqn (8), Eqn (36) still includes $\mathbf{t}^w$ and $\overset{s\to w}{\mathbf{T}}$, which are expressions involving averages of microscale quantities that are only accessible if a microscale solution exists.

With microscale simulations, we are able to directly examine each term in Eqns (8) and (36) and estimate the Stokes limit for each of the domains. Figure 3 depicts the component in the primary direction of flow for the terms in the macroscale conservation equation. The time derivative of all solutions is zero as only steady-state simulations were considered. As the Re increases, the values of each term in Eqn (36) (note, we depict $\mathbf{t}^{\overline{\overline{w}}}$) remain relatively constant until $\mathrm{Re} \approx 1$ for each of the domains. Since we solved the slightly-compressible Navier-Stokes equations at the microscale, the applicability of Eqn (36), as opposed to Eqn (8), can be determined as a function of Re. Using a maximum allowable residual of 10^{-8}, the Stokes equation is valid for $\mathrm{Re} \leq \mathrm{Re}_s = 0.15$, 0.17, and 0.075, for the uniform, log-normal, and ellipsoid domains, respectively. At and above Re_s, the nonlinear advective transport term, which does not appear in the Stokes equation, becomes significant. Therefore, the macroscale momentum equation given as Eqn (36) is only valid up to Re_s for errors on the order of 10^{-8}.

To generate a generally applicable approximate macroscale solution, an approximation to $\mathbf{t}^w$, or $\mathbf{t}^{\overline{\overline{w}}}$, and $\overset{s\to w}{\mathbf{T}}$ are required, which must be formulated in terms of accessible macroscale quantities, which can be accomplished using the SEI given by Eqn (33). This equation includes two flux-force pairs. The independent forces are $\mathbf{d}^{\overline{\overline{w}}}$ and $\mathbf{v}^{\overline{w}}$, and the independent fluxes are the terms that multiply each of these forces. Any valid closure approximation must satisfy the inequality given by Eqn (33). While valid closure approximations are not unique, the objective is to approximate the finer scale detail that is unknown as accurately as needed for the intended purposes of the model. Because of the independence of the fluxes and forces, each of these flux-force pairs can be considered independently [23].

Because $\mathbf{d}^{\overline{\overline{w}}}$ depends upon $\nabla\mathbf{v}^{\overline{w}}$, an approximation can be made that the flux-force pair involving $\mathbf{d}^{\overline{\overline{w}}}$ is of a higher order, thus less important, than the flux-force pair involving $\mathbf{v}^{\overline{w}}$. This is akin to dropping higher order terms in a Taylor series expansion. Consider the first flux-pair, which requires

$$\left(\epsilon^{\overline{\overline{w}}}\mathbf{t}^{\overline{\overline{w}}} + \epsilon^{\overline{\overline{w}}}p^w\mathbf{I}\right):\mathbf{d}^{\overline{\overline{w}}} \geq 0\ . \tag{37}$$

A zero-order approximation is the simplest possible approximation that satisfies this equation [20]. Such an approximation leads to [23, Eqn (9.74)]

$$\left(\epsilon^{\overline{\overline{w}}}\mathbf{t}^{\overline{\overline{w}}} + \epsilon^{\overline{\overline{w}}}p^w\mathbf{I}\right):\mathbf{d}^{\overline{\overline{w}}} = 0\ , \tag{38}$$

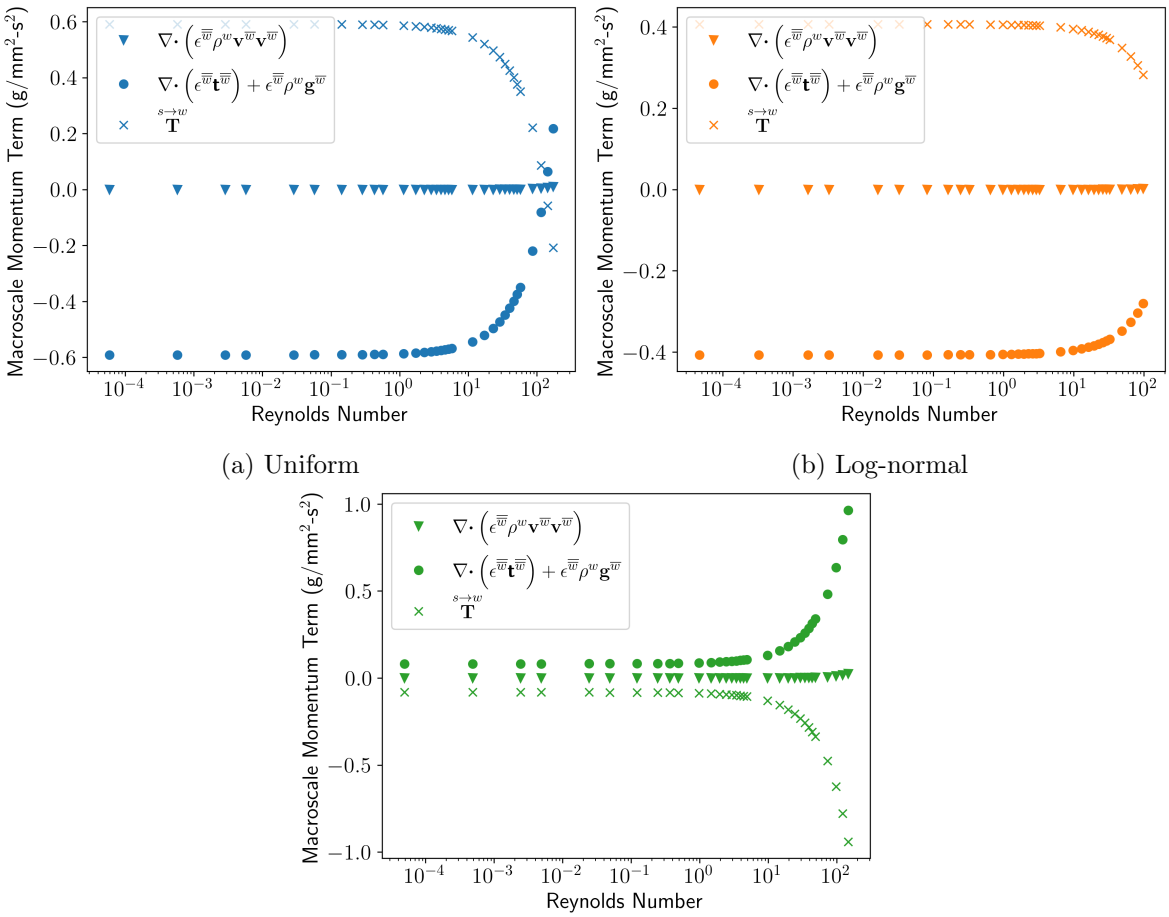

(a) Uniform

(b) Log-normal

(c) Ellipsoid

Figure 3: Comparison of terms in Eqn (8) as calculated from microscale precursors. Values shown are in the primary direction of flow which is opposite the direction of gravity.

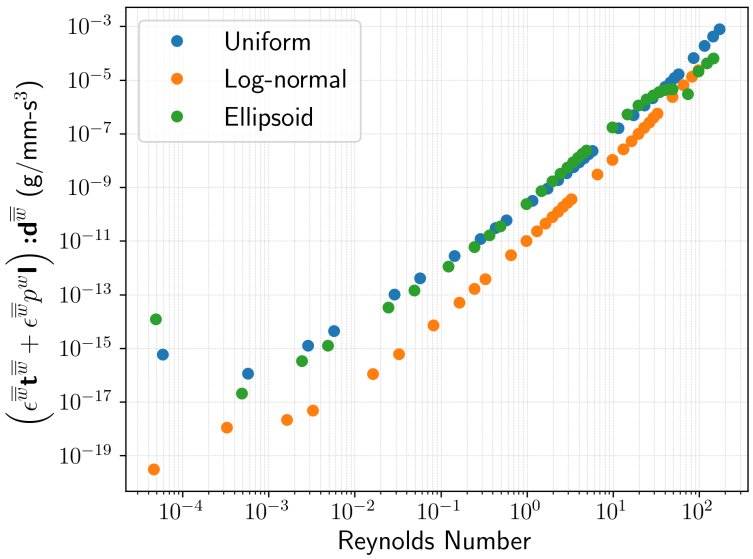

Figure 4: Evaluation of macroscale stress tensor closure relation Eqn (38).

which can be satisfied by

$$\mathbf{t}^{\overline{\overline{w}}} = -p^w\mathbf{I}\,. \tag{39}$$

Eqn (39) satisfies the SEI and ensures consistency with the second-law of thermodynamics, as any valid closure relation must. Recalling Eqns (3) and (9), this closure approximation implies macroscopically inviscid flow, which is consistent with the observations of flow at the macroscale.

From the microscale simulations, we are able to quantify the error introduced with the zero-order macroscale closure approximation. Figure 4 depicts the evaluation of Eqn (38) for the three simulation domains where the error from the closure approximation is the deviation from zero. The error associated with this approximation is $\ll 10^{-8}$ at $\mathrm{Re} < \mathrm{Re}_s$, which validates this approximation. However, alternative closure approximation approaches may be needed for larger Re.

The second condition that must be satisfied based upon Eqn (33) is

$$\left[\nabla\left(\epsilon^{\overline{\overline{w}}}p^w\right) - \epsilon^{\overline{\overline{w}}}\rho^w\nabla\left(\mu^{\overline{w}} + \psi^{\overline{w}}\right) - \epsilon^{\overline{\overline{w}}}\rho^w\mathbf{g}^{\overline{w}} - \overset{s\to w}{\mathbf{T}}\right]\cdot\mathbf{v}^{\overline{w}} \geq 0\,, \tag{40}$$

which is assumed to be the dominant entropy-producing flux-force pair for this problem. The force is $\mathbf{v}^{\overline{w}}$ and the flux is the preceding term that is dotted with this force. Note that $\overset{s\to w}{\mathbf{T}}$ is a component of this flux and involves generally inaccessible microscale quantities as shown in Eqn (10), and appears in Eqn (36). A useful closure approximation would thus provide an approximation for $\overset{s\to w}{\mathbf{T}}$ in terms of macroscale variables that are accessible. Note that the flux quantity being approximated is a vector.

The simplest approximation consistent with Eqn (40) and of higher order than the approximation used to approximate $\mathbf{t}^{\overline{\overline{w}}}$ is a first-order conjugate flux-force expression of the form [23, Eqn (9.77)]

$$\nabla\left(\epsilon^{\overline{\overline{w}}}p^w\right) - \epsilon^{\overline{\overline{w}}}\rho^w\nabla\left(\mu^{\overline{w}} + \psi^{\overline{w}}\right) - \epsilon^{\overline{\overline{w}}}\rho^w\mathbf{g}^{\overline{w}} - \overset{s\to w}{\mathbf{T}} = \hat{R}^w\mathbf{v}^{\overline{w}}\,, \tag{41}$$

where $\hat{R}^w$ is a non-negative scalar resistance coefficient assumed to depend upon fluid and

solid properties. Substituting Eqn (41) into Eqn (40) yields

$$\hat{R}^w \mathbf{v}^{\overline{w}} \cdot \mathbf{v}^{\overline{w}} \geq 0 \,, \tag{42}$$

which is satisfied for all $\mathbf{v}^{\overline{w}}$ provided $\hat{R}^w > 0$, which is a requirement of the resistance coefficient.

It can be shown using microscale simulation methods of the sort used in this work that the flux vector in Eqn (41) need not be colinear with $\mathbf{v}^{\overline{w}}$, which is a definition of an anisotropic porous medium [15]. An anisotropic generalization of Eqn (41) is

$$\nabla \left(\epsilon^{\overline{\overline{w}}} p^w \right) - \epsilon^{\overline{\overline{w}}} \rho^w \nabla \left(\mu^{\overline{w}} + \psi^{\overline{w}} \right) - \epsilon^{\overline{\overline{w}}} \rho^w \mathbf{g}^{\overline{w}} - \overset{s \to w}{\mathbf{T}} = \hat{\mathbf{R}}^w \cdot \mathbf{v}^{\overline{w}} \,, \tag{43}$$

where $\hat{\mathbf{R}}^w$ is a second-rank, symmetric, positive-definite resistance tensor assumed to depend upon fluid and solid properties. It follows then that

$$\mathbf{v}^{\overline{w}} \cdot \hat{\mathbf{R}}^w \cdot \mathbf{v}^{\overline{w}} \geq 0 \,, \tag{44}$$

which is also consistent with Eqn (40), proving Eqn (43) is a permissible closure approximation.

Eqn (43) can be rearranged to solve for the inter-entity transfer of momentum term giving

$$\nabla \left(\epsilon^{\overline{\overline{w}}} p^w \right) - \epsilon^{\overline{\overline{w}}} \rho^w \nabla \left(\mu^{\overline{w}} + \psi^{\overline{w}} \right) - \epsilon^{\overline{\overline{w}}} \rho^w \mathbf{g}^{\overline{w}} - \hat{\mathbf{R}}^w \cdot \mathbf{v}^{\overline{w}} = \overset{s \to w}{\mathbf{T}} \,. \tag{45}$$

Substituting Eqns (39) and (45) into Eqn (36) yields an alternative macroscale form of a Stokes-flow approximation in terms of all macroscale quantities

$$-\epsilon^{\overline{\overline{w}}} \rho^w \nabla \left(\mu^{\overline{w}} + \psi^{\overline{w}} \right) = \hat{\mathbf{R}}^w \cdot \mathbf{v}^{\overline{w}} \,. \tag{46}$$

Note that this macroscale Stokes-flow equation, Eqn (46), involves the gradient of the sum of chemical and gravitational potentials. When the sum of these potentials is constant, such as would be the case at equilibrium, then $\mathbf{v}^{\overline{w}}$ must vanish.

Alternative forms of Eqn (46) can be formulated as well. For example, $\mu^{\overline{w}}$ can be related to p^w by the macroscale variant of the Gibbs-Duhem equation [23, Eqn (7.33)], and $\psi^{\overline{w}}$ can be related to $\mathbf{g}^{\overline{w}}$ to yield [22, 23]

$$\epsilon^{\overline{\overline{w}}} \left(\nabla p^w - \rho^w \mathbf{g}^{\overline{w}} \right) - \left\langle \nabla \left(p_w - p^w \right) \right\rangle_{\Omega_w, \Omega} + \left\langle \rho_w \nabla \left(\mu_w + \psi_w - \mu^{\overline{w}} - \psi^{\overline{w}} \right) \right\rangle_{\Omega_w, \Omega} = \hat{\mathbf{R}}^w \cdot \mathbf{v}^{\overline{w}} \,. \tag{47}$$

This form includes the microscale quantities that are commonly ignored. The ability to uncover the often ignored terms highlights the benefit of the explicit connection across spatial scales.

Classically, the form of a macroscale model and closure relations are posited to produce a solvable model. An extension to Darcy's law [12] is often used and written in the form

$$\mathbf{q}^{\overline{\overline{w}}} = \epsilon^{\overline{\overline{w}}} \mathbf{v}^{\overline{w}} = -\hat{K} \nabla h^w \tag{48}$$

or in tensor form as

$$\mathbf{q}^{\overline{\overline{w}}} = \epsilon^{\overline{\overline{w}}} \mathbf{v}^{\overline{w}} = -\hat{\mathbf{K}} \cdot \nabla h^w \,, \tag{49}$$

where $\mathbf{q}^{\overline{\overline{w}}}$ is a specific discharge vector, $\hat{K}$ is a scalar hydraulic conductivity, h is hydraulic head, and $\hat{\mathbf{K}}$ is a hydraulic conductivity tensor [20]. Because Eqn (48), or Eqn (49), is an equation for $\mathbf{q}^{\overline{\overline{w}}}$, it is an approximation of the momentum equation given by Eqn (8), but this loose connection is not sufficient to illustrate how this equation could be derived in the absence of the seminal work of Darcy, and the assumptions and limitation of this approach.

With the microscale simulation results, we determine $\hat{R}^w$ for each domain by performing a least squares minimization where only simulations where $\mathrm{Re} < \mathrm{Re}_s$ were included resulting in 6 simulations per domain (Table 2). The error is defined as the residual of Eqn (41), where the term on the right of the equal sign was brought to the left, and the fit $\hat{R}^w$ was used, given as

$$R = \nabla\left(\epsilon^{\overline{w}} p^w\right) - \epsilon^{\overline{w}}\rho^w\nabla\left(\mu^{\overline{w}} + \psi^{\overline{w}}\right) - \epsilon^{\overline{w}}\rho^w\mathbf{g}^{\overline{w}} - \overset{s\to w}{\mathbf{T}} - \hat{R}^w\mathbf{v}^{\overline{w}} \,. \tag{50}$$

The mean squared error (MSE) is defined as

$$\mathrm{MSE} = \frac{1}{n}\sum_i^n R_i^2 \,, \tag{51}$$

and the maximum absolute error (MAE) as

$$\mathrm{MAE} = \max_i |R_i| \,. \tag{52}$$

where i is the residual for each simulation where $\mathrm{Re} < \mathrm{Re}_s$ and $n = 6$. Note that the expected solution is zero as the error measure is defined as the residual. The errors for this approximation are orders of magnitude larger as compared to our other closure approximation (Figure 4), which was expected based on the order of the velocity terms. Higher order models can be posed to further minimize the error, however, this approach has been applied successfully and the maximum errors with our macroscale approximations are of the same order as our tolerance.

Table 2: Estimation of $\hat{R}^w$ in the Primary Direction of Flow for $\mathrm{Re} \leq \mathrm{Re}_s$

Property	Uniform	Log-normal	Ellipsoid
$\hat{R}^w$ (g/mm^3-s)	4.17×10^{-2}	1.43×10^{-2}	3.96×10^{-2}
MSE	3.82×10^{-9}	4.99×10^{-9}	1.04×10^{-8}
MAE	1.93×10^{-8}	2.64×10^{-8}	4.33×10^{-8}

4.4 Transition Flow

As Re approaches unity, fluid behavior changes as can be seen from Figure 3 and described in [11]. Table 3 contains results for when a first-order approximation (Eqn 41) is used for all 32 simulations per domain where Re ranged from $10^{-8} - 10^2$. From these results, it is clear that while this approximation was valid in the Stokes regime, the errors in the transition region are orders of magnitude higher.

Table 3: Estimation of $\hat{R}^w$ in the Primary Direction of Flow for All Simulations

Property	Uniform	Log-normal	Ellipsoid
$\hat{R}^w$ (g/mm^3-s)	4.58×10^{-2}	1.54×10^{-2}	4.46×10^{-2}
MSE	1.57×10^{-3}	2.04×10^{-4}	1.89×10^{-3}
MAE	3.01×10^{-2}	3.91×10^{-3}	3.50×10^{-2}

The approach used to derive the SEI ensures that Eqn (33) is also valid at describing entropy production for higher Re flow, commonly known as transition or non-Darcy flow. We can therefore re-assess the closure approximation made in Eqn (41) to extend the applicability

of our closure relation to a more generic system. As the first-order approximation has been shown to be insufficient, we posit a second-order closure such that

$$\nabla\left(\epsilon^{\overline{\overline{w}}}p^{w}\right)-\epsilon^{\overline{\overline{w}}}\rho^{w}\nabla\left(\mu^{\overline{w}}+\psi^{\overline{w}}\right)-\epsilon^{\overline{\overline{w}}}\rho^{w}\mathbf{g}^{\overline{w}}-\overset{s\rightarrow w}{\mathbf{T}}=\hat{R}^{w}\mathbf{v}^{\overline{w}}+\hat{k}^{w}|\mathbf{v}^{\overline{w}}|\mathbf{v}^{\overline{w}}\,, \tag{53}$$

which is similar to the Forchheimer extension of Darcy's Law [16] and includes $\hat{k}^{w}$, an additional resistance coefficient. As with the first-order approximation, the restrictions on $\hat{R}^{w}$ still apply, Eqn (42), and we introduce a new restriction on $\hat{k}^{w}$, such that

$$\hat{k}^{w}|\mathbf{v}^{\overline{w}}|\mathbf{v}^{\overline{w}}\cdot\mathbf{v}^{\overline{w}}\geq 0\,. \tag{54}$$

It is important to note here that models of any form are permissible such that they obey the conditions set by the entropy inequality. We suggest zero, first, and second order models out of simplicity and their natural connection to familiar models. New data-driven modeling approaches have been shown to pair well with the TCAT methodology to better incorporate physics into closure relations [9].

To assess the performance of this higher order closure relation, we again use the microscale simulation results and perform a least squares minimization to determine $\hat{R}^{w}$ and $\hat{k}^{w}$ in the primary direction of flow (Table 4). For this case, we define the error as the residual of Eqn (53) after arranging the equation to be equal to zero. While the errors in this second-order approximation are larger than our specified allowable tolerance, both error metrics are at least an order of magnitude lower than the first-order approximation. If this error was deemed too large for the intended applications of the derived macroscale model, alternative closure approximations could further be posited.

Table 4: Estimation of $\hat{R}^{w}$ and $\hat{k}^{w}$ in the Primary Direction of Flow

Property	Uniform	Log-normal	Ellipsoid
$\hat{R}^{w}$ (g/mm^3-s)	4.06×10^{-2}	1.40×10^{-2}	3.90×10^{-2}
$\hat{k}^{w}$ (g/mm^3-s)	4.39×10^{-4}	2.75×10^{-4}	4.71×10^{-4}
MSE	9.94×10^{-5}	1.30×10^{-5}	3.03×10^{-5}
MAE	1.42×10^{-3}	1.89×10^{-4}	3.65×10^{-4}

The closure approximation of the force-flux pair involving $\mathbf{d}^{\overline{\overline{w}}}$ was assumed to be higher order due to its dependence on $\nabla\mathbf{v}^{\overline{w}}$. However, with the second-order closure for our other term, the approximations are of the same magnitude at high Re, where we evaluate the closure relationships with the best fit parameters (Figure 5). Extension of the derived macroscale model to higher Re would require inspection of the zero-order closure approximation.

5 Why Bother?

A question posed in the title of this work is why bother with TCAT? Motivating this question is the seeming complexity of the approach, which relies upon conservation and balance equations for phases, interfaces, common curves, and common points; thermodynamics; multiple coordinate systems at the microscale and larger scales; generalized functions; averaging operators; multiscale theorems; calculus of variations; differential and integral geometry; topology; and evolution equations—yielding entropy inequalities that span multiple pages of heavily adorned symbols relied upon to produce closed models. The motivation for each of these components could and has been discussed [e.g., 19, 21, 23, 26, 34, 35, 37], but such a discussion does not resolve the question. The complexity of the method is due to our inability

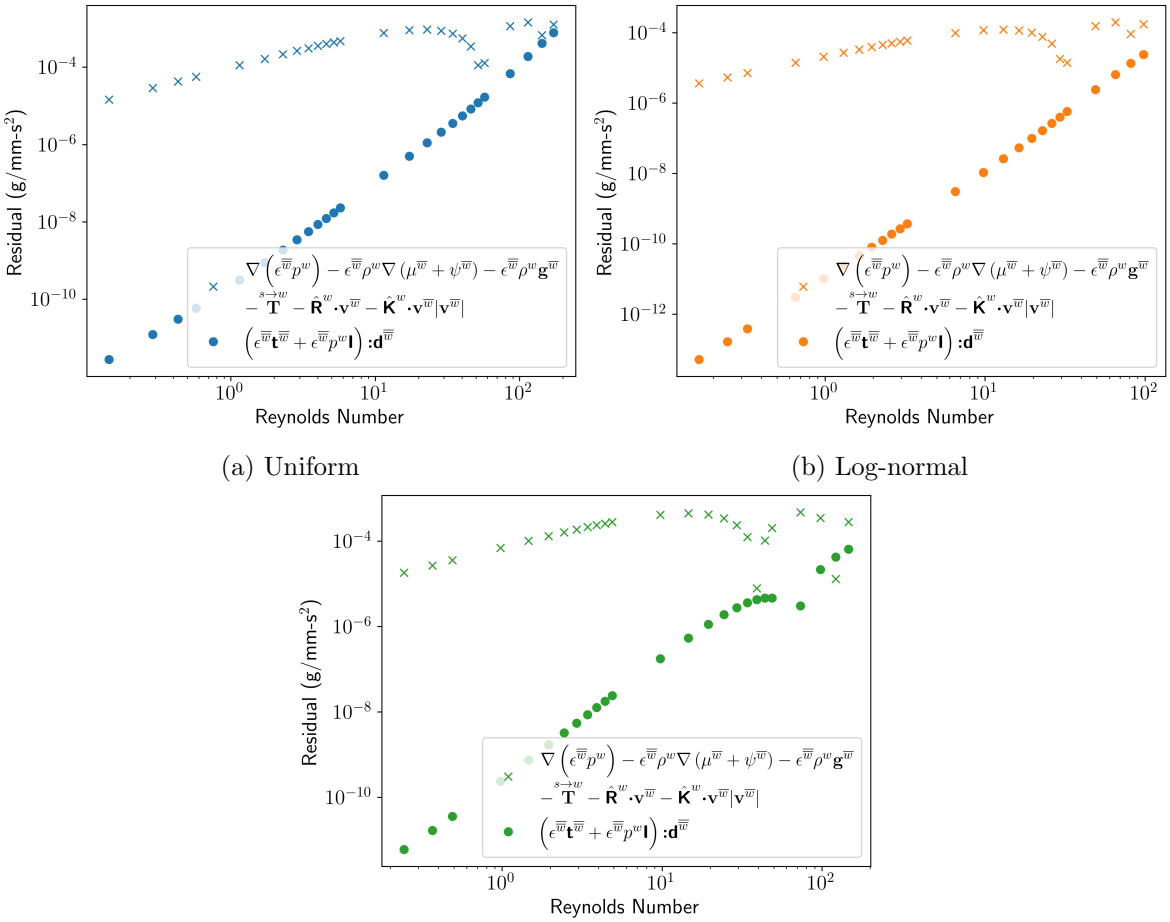

(a) Uniform

(b) Log-normal

(c) Ellipsoid

Figure 5: Comparison of errors for closure approximations for transitional flow. Values shown are in the primary direction of flow, when applicable.

to accomplish the goal of building rigorous, high-fidelity, scale-consistent models for complex systems using simpler approaches. However, theoretical elegance is insufficient motivation for most researchers and practitioners to expend the effort needed to understand all of the details of TCAT, especially if the benefits of doing so are not compelling in light of the required effort.

Our answer to this question can be summarized as: the current state of TCAT modeling enables (1) the formulation of models that are consistent across length scales, thermodynamically constrained, of variable and potentially high fidelity; and (2) the generation and application of a wide variety of new models that rely upon existing theoretical results without the need to understand the details involved in formulating these results. Simply put, TCAT is a compelling approach with many benefits and most of the heavy lifting has already been done. Some additional details supporting this answer are warranted, and we comment on scale consistency, the generation of new models, the replacement of empiricism with theory, and available components of potential use.

TCAT ensures consistency across length scales, which can be leveraged to advantage as shown in this work. By consistency we mean that all macroscale quantities are precisely defined in terms of microscale quantities. This includes thermodynamic quantities (e.g., pressure, chemical potential, temperature) a feature that distinguishes TCAT from other methods that assume a thermodynamic relation at the macroscale and thus leaves these intrinsic variables undefined for purposes of experimental study. This connection was used in this work by computing a microscale solution, applying an available averaging operator and change of scale theorems to in turn compute all terms in an essentially exact macroscale equation. This enabled verification of the theoretical results, evaluation of the accuracy of the microscale simulations, parameter estimation of macroscale closure relations, and a quantitative assessment of the accuracy of approximate macroscale closure relations. When the closure approximation introduces significant error, the precise term contributing to this error can be shown, and improved approximations deduced as needed and possible based upon the derived EI. This approach is in sharp contrast with phenomenological approaches, which might fit data in certain cases, fail in other cases, and might not even be thermodynamically feasible [38, 41]. The approach used herein could be applied to TCAT models in general not just the model considered in this work, which is a powerful approach for model evaluation and validation.

The model investigated in this work was simple to highlight some basic notions of TCAT. The closure relations investigated are essentially identical to what have been used for decades for this case [3]. TCAT can be applied to generate new models that do not exist. For example, TCAT has been used to derive models to describe the flow of non-Newtonian fluids through porous media [8, 9]. These example model extensions leverage an available TCAT EI and the connection across scales to produce models that can predict non-Newtonian flow based only on medium characteristics and the rheological properties of the fluid. Two-fluid flow through porous media is another class of model in which TCAT approaches have produced novel model formulations [10, 30], with much additional work possible in this area building upon the existing TCAT modeling components and compelling reasons to pursue such work. Other examples exist as well that might be considered low-hanging fruit, such as non-dilute transport in a single-fluid system [52].

A cornerstone of TCAT approaches is the replacement of empirical phenomenological relations with theoretically-based model components where possible. Some examples of such approaches can be used to illustrate the notion. An element of TCAT modeling is the development of an EI. EI's are used to deduce conditions that must be met for a closure relation to be permissible or consistent with the second law of thermodynamics. Closure relations consistent with an EI are non-unique and even if a closure relation is known, one must still determine the parameters that arise in the relation. In certain situations, parameters can be determined

a priori for TCAT models [36]. Other features unique to TCAT models, overlooked or incorrectly proposed in other approaches, include the formulation of closure relations of evolution equations for geometric properties based upon averaging theorems [21, 23, 26], and the use of integral geometry and topology to deduce state equations for two-fluid porous medium systems [27, 37].

Many available components of TCAT models already exist and may be used without re-derivation. These components include microscale and macroscale conservation, balance, thermodynamic, and potential equations for phases, interfaces, and common curves; entropy inequalities for single- and two-fluid systems; equilibrium conditions at the microscale and macroscale; precise definitions of macroscale quantities in terms of microscale quantities and averaging operators; evolution equations for phases and interfaces; and a state equation for two-fluid system [23, 37, 47]. The example provided in this work illustrates how such available modeling components can be used, other examples are available in the literature [e.g., 8, 9, 39].

6 Summary and Conclusions

While the mathematical complexity can be daunting, the TCAT methodology offers a rigorous approach for evaluating microscale simulations, deriving exact macroscale equations, and evaluating macroscale closure relations. Paired with microscale simulations, the errors associated with the necessary approximations can be quantified. In this work, we examined the case of single-fluid flow in a porous medium. From the presumed exact microscale governing equations, an exact macroscale model was formulated and validated with computational fluid dynamic simulations of the slightly-compressible Navier-Stokes equations. As TCAT is consistent across all scales, macroscale variables were calculated from microscale simulations. With this information, closure relations that do not contain any microscale variables were posited and the microscale simulation results were used to assess the approximations. The TCAT methodology provides a fundamental approach for deriving larger scale models that can be assessed with microscale simulations. The approaches illustrated in this work apply to all systems for which TCAT entropy inequalities have been derived [23, 31, 47, 48, 52]. TCAT methods are sufficiently developed that abundant opportunities for model advancement and validation exist based upon the extension of existing results.

7 Acknowledgments

This work was supported by National Institute of Environmental Health Sciences grant P42ES031007. This work was also supported by the Extreme Science and Engineering Discovery Environment (XSEDE), National Science Foundation grant number ACI-1548562. Bridges-2 at the Pittsburgh Supercomputing Center and Expanse at the San Diego Supercomputing Center (CTS200041) were used for the simulations. The authors acknowledge the efforts of two anonymous peer reviewers for their comprehensive, careful, detailed, and constructive comments, which helped us to improve this work.

Data availability

All code used and data generated in this work are available at `https://github.com/tmweigand/tcat-1p`.

Author Contributions

TMW: Conceptualization, Software, Writing—Original Draft, Writing—Review & Editing, Visualization.
WGG: Conceptualization, Methodology, Writing—Original Draft, Writing—Review & Editing.
CTM: Conceptualization, Methodology, Writing—Original Draft, Writing—Review & Editing, Funding acquisition.

A Averaging Operator and Theorems

For completeness, we include the definitions of the averaging theorems used in this work as well as the definition of the averaging operator. For complete details refer to [23, 24]. The averaging operator is defined as [23, Eqn (6.1)]

$$\langle f_\alpha \rangle_{\Omega_\beta,\Omega_\gamma,W} = \frac{\int\limits_{\Omega_\beta} W f_\alpha \,\mathrm{d}\mathfrak{r}}{\int\limits_{\Omega_\gamma} W \,\mathrm{d}\mathfrak{r}} \,. \tag{55}$$

The transport theorem used to convert microscale temporal derivatives to macroscale temporal derivatives, formally defined as T[3(3,0),0], is [23, Eqn (B.17)]

$$\int\limits_{\Omega_w} \frac{\partial f}{\partial t} \,\mathrm{d}\mathfrak{r} = \frac{\partial}{\partial t} \int\limits_{\Omega_w} f \,\mathrm{d}\mathfrak{r} - \int\limits_{\Omega_{ws}} \mathbf{n}\cdot\mathbf{w} f \,\mathrm{d}\mathfrak{r} \,. \tag{56}$$

The divergence theorem, formally given as D[3(3,0),0] is [23, Eqn (B.12)]

$$\int\limits_{\Omega_w} \nabla\cdot\mathbf{f} \,\mathrm{d}\mathfrak{r} = \nabla\cdot \int\limits_{\Omega_w} \mathbf{f} \,\mathrm{d}\mathfrak{r} - \int\limits_{\Omega_{ws}} \mathbf{n}\cdot\mathbf{f} \,\mathrm{d}\mathfrak{r} \,, \tag{57}$$

and the gradient theorem, or G[3(3,0),0], is [23, Eqn (B.13)]

$$\int\limits_{\Omega_w} \nabla f \,\mathrm{d}\mathfrak{r} = \nabla \int\limits_{\Omega_w} f \,\mathrm{d}\mathfrak{r} - \int\limits_{\Omega_{ws}} \mathbf{n} f \,\mathrm{d}\mathfrak{r} \,. \tag{58}$$

Nomenclature

Greek Symbols

α	Entity qualifier
$\hat{\beta}$	Compressibility of w phase
ϵ	Porosity
$\epsilon^{\overline{\overline{w}}}$	Volume fraction of w phase
$\epsilon^{\overline{\overline{ws}}}$	Specific surface area of the ws interface
η	Entropy per volume

γ^{ws} Interfacial tension of the ws interface

Γ Domain boundary

λ Lagrange multiplier

Λ Entropy production rate density

μ Chemical potential

$\hat{\mu}$ Dynamic viscosity

Ω Domain

ψ Gravitational potential

ρ Density

$\boldsymbol{\tau}$ Viscous stress tensor

θ Temperature

Roman Symbols

$\mathbf{d}$ Rate of strain tensor

E Internal energy per volume

$\mathcal{E}_*^{\overline{\overline{\alpha}}}$ Conservation of energy equations

F Force

$\mathbf{g}$ Gravitational acceleration vector

$\mathbf{G}^{ws}$ Geometric orientation tensor for the ws interface

$\mathcal{G}_*^{\overline{\overline{\alpha}}}$ Potential energy equations

$\mathbf{h}$ Position vector

$\mathbf{I}$ Identity tensor

$\mathfrak{I}_P$ Index set of phases

J Flux

J_s^{ws} Twice the mean curvature of the ws interface

$\hat{k}^w$ Scalar resistance coefficient

$\hat{K}$ Scalar hydraulic conductivity

ℓ Sauter mean diameter

m Mass flow rate

$\mathcal{M}_*^{\overline{\overline{\alpha}}}$ Conservation of mass equations

$\mathbf{n}_w$ Unit normal vector pointing outward from w phase

p Pressure

$\boldsymbol{\mathcal{P}}_*^{\overline{\overline{\alpha}}}$ Conservation of momentum equations

$\mathbf{q}$ Specific discharge vector

$\hat{R}$ Ideal gas constant

$\hat{R}^w$ Scalar resistance coefficient

$\mathcal{S}$ Entropy balance equation

t Time

$\mathbf{t}$ Stress tensor

$\overset{s\to w}{\mathbf{T}}$ Momentum exchange from s phase to w phase

$\mathcal{T}_*^{\overline{\overline{\alpha}}}$ Thermodynamic equations

$\mathcal{T}_{\mathcal{G}*}^{\overline{\overline{\alpha}}}$ Potential energy equations

$\mathbf{v}$ Velocity vector

References

[1] V. Baranau and U. Tallarek. Another resolution of the configurational entropy paradox as applied to hard spheres. *The Journal of Chemical Physics*, 147(22):224503, 2017. doi: 10.1063/1.4999483.

[2] I. Battiato, P. T. Ferrero, D. O'Malley, C. T. Miller, P. S. Takhar, F. J. Valdés-Parada, and B. D. Wood. Theory and applications of macroscale models in porous media. *Transport in Porous Media*, 130(1):5–76, 2019. doi: 10.1007/s11242-019-01282-2.

[3] J. Bear. *Dynamics of Fluids in Porous Media*. Elsevier, New York, 1972.

[4] J. Bear. *Modeling Phenomena of Flow and Transport in Porous Media*. Springer International, Switzerland, 2018.

[5] J. Bear and L. G. Fel. A phenomenological approach to modeling transport in porous media. *Transport in Porous Media*, 92(3):649–665, 2012. doi: 10.1007/s11242-011-9926-3.

[6] L. S. Bennethum and J. H. Cushman. Multiphase, multicomponent theory for multiscale swelling systems with interfaces. Part II: Constitutive theory. *International Journal of Engineering Science*, 34(2):147–169, 1996.

[7] R. B. Bird, W. E. Stewart, and E. N. Lightfoot. *Transport Phenomena*. John Wiley & Sons, Inc., revised 2nd edition, 2007.

[8] C. A. Bowers and C. T. Miller. Generalized Newtonian fluid flow in porous media. *Physical Review Fluids*, 6(12):123302, 2021. doi: 10.1103/PhysRevFluids.6.123302.

[9] C. A. Bowers and C. T. Miller. Modeling flow of Carreau fluids in porous media. *Physical Review E*, 108(6):065106, 2023.

[10] K. Bruning and C. T. Miller. Toward a new generation of two-fluid flow models based on the thermodynamically-constrained averaging theory. *Water*, 11(11), 2019. doi: 10.3390/w11112260.

[11] K. Chaudhary, M. B. Cardenas, W. Deng, and P. C. Bennett. The role of eddies inside pores in the transition from Darcy to Forchheimer flows. *Geophysical Research Letters*, 38(24), 2011. doi: https://doi.org/10.1029/2011GL050214.

[12] H. Darcy. *Les Fontaines Publiques de la Ville de Dijon*. Dalmont, Paris, 1856.

[13] H. Darcy. Determination of the laws of flow of water through sand. In R. A. Freeze and W. Back, editors, *Physical Hydrology*. Hutchinson Ross, Stroudsburg, PA, 1983.

[14] M. Dentz, J. J. Hidalgo, and D. Lester. Mixing in porous media: Concepts and approaches across scales. *Transport in Porous Media*, 146(1):5–53, 2023. doi: 10.1007/s11242-022-01852-x.

[15] A. L. Dye, J. E. McClure, C. T. Miller, and W. G. Gray. Description of non-Darcy flows in porous medium systems. *Physical Review E*, 87(3), 2013. doi: 10.1103/PhysRevE.87.033012.

[16] P. H. Forchheimer. Wasserbewegun durch Boden. *Zeitschrift des Vereines Deutscher Ingenieure*, 45:1782–1788, 1901.

[17] J. B. J. Fourier. *Théorie Analytique de la Chaleur*. Firmin Didot, 1822.

[18] R. A. Freeze and J. A. Cherry. *Groundwater*. Prentice-Hall, Inc., Englewood Cliffs, NJ, 1979.

[19] W. G. Gray and C. T. Miller. Thermodynamically constrained averaging theory approach for modeling flow and transport phenomena in porous medium systems: 1. Motivation and overview. *Advances in Water Resources*, 28(2):161–180, 2005. doi: 10.1016/j.advwatres.2004.09.005.

[20] W. G. Gray and C. T. Miller. Thermodynamically constrained averaging theory approach for modeling flow and transport phenomena in porous medium systems: 3. Single-fluid-phase flow. *Advances in Water Resources*, 29(11):1745–1765, 2006. doi: 10.1016/j.advwatres.2006.03.010.

[21] W. G. Gray and C. T. Miller. Thermodynamically constrained averaging theory approach for modeling flow and transport phenomena in porous medium systems: 8. Interface and common curve dynamics. *Advances in Water Resources*, 33(12):1427–1443, 2010. doi: 10.1016/j.advwatres.2010.01.010.

[22] W. G. Gray and C. T. Miller. On the algebraic and differential forms of Darcy's equation. *Journal of Porous Media*, 14(1):33–50, 2011.

[23] W. G. Gray and C. T. Miller. *Introduction to the Thermodynamically Constrained Averaging Theory for Porous Medium Systems*. Springer, Switzerland, 2014. doi: 10.1007/978-3-319-04010-3.

[24] W. G. Gray, A. Leijnse, R. L. Kolar, and C. A. Blain. *Mathematical tools for changing spatial scales in the analysis of physical systems*. CRC Press, 2000.

[25] W. G. Gray, C. T. Miller, and B. A. Schrefler. Averaging theory for description of environmental problems: What have we learned? *Advances in Water Resources*, 51:123–138, 2013. doi: 10.1016/j.advwatres.2011.12.005.

[26] W. G. Gray, A. L. Dye, J. E. McClure, L. J. Pyrak-Nolte, and C. T. Miller. On the dynamics and kinematics of two-fluid-phase flow in porous media. *Water Resources Research*, 51(7):5365–5381, 2015. doi: 10.1002/2015wr016921.

[27] W. G. Gray, K. Bruning, and C. T. Miller. Non-hysteretic functional form of capillary pressure in porous media. *Journal of Hydraulic Research*, 57(6):747–759, 2019. doi: 10.1080/00221686.2019.1671520.

[28] S. M. Hassanizadeh and W. G. Gray. General conservation equations for multi-phase systems: 1. Averaging procedure. *Advances in Water Resources*, 2(3):131–144, 1979.

[29] U. Hornung. *Homogenization and Porous Media*. Springer, 1997.

[30] A. S. Jackson, C. T. Miller, and W. G. Gray. Thermodynamically constrained averaging theory approach for modeling flow and transport phenomena in porous medium systems: 6. Two-fluid-phase flow. *Advances in Water Resources*, 32(6):779–795, 2009. doi: 10.1016/j.advwatres.2008.11.010.

[31] A. S. Jackson, I. Rybak, R. Helmig, W. G. Gray, and C. T. Miller. Thermodynamically constrained averaging theory approach for modeling flow and transport phenomena in porous medium systems: 9. Transition region models. *Advances in Water Resources*, 42:71–90, 2012. doi: 10.1016/j.advwatres.2012.01.006.

[32] G. A. Maugin. *The Thermomechanics of Nonlinear Irreversible Behaviors: An Introduction*. World Scientific Press, Singapore, 1999.

[33] R. M. Maxwell, L. E. Condon, and S. J. Kollet. A high-resolution simulation of groundwater and surface water over most of the continental us with the integrated hydrologic model ParFlow v3. *Geoscientific Model Development*, 8(3):923–937, 2015. doi: 10.5194/gmd-8-923-2015.

[34] C. T. Miller and W. G. Gray. Thermodynamically constrained averaging theory approach for modeling flow and transport phenomena in porous medium systems: 2. Foundation. *Advances in Water Resources*, 28(2):181–202, 2005. doi: 10.1016/j.advwatres.2004.09.006.

[35] C. T. Miller and W. G. Gray. Hydrogeological research, education, and practice: A path to future contributions. *Journal of Hydrologic Engineering*, 13(1):7–12, 2008. doi: 10.1061/(Asce)1084-0699(2008)13:1(7).

[36] C. T. Miller, F. J. Valdés-Parada, and B. D. Wood. A pedagogical approach to the thermodynamically constrained averaging theory. *Transport in Porous Media*, 119:585–609, 2017. doi: 10.1007/s11242-017-0900-6.

[37] C. T. Miller, K. Bruning, C. L. Talbot, J. E. McClure, and W. G. Gray. Non-hysteretic capillary pressure in two-fluid porous media: Definition, evaluation, validation, and dynamics. *Water Resources Research*, 55:6825–6849, 2019. doi: 10.1029/2018WR024586.

[38] C. T. Miller, W. G. Gray, C. E. Kees, I. V. Rybak, and B. J. Shepherd. Modelling sediment transport in three-phase surface water systems. *Journal of Hydraulic Research*, 57(4):439–463, 2019. doi: 10.1080/00221686.2019.1581673.

[39] C. T. Miller, W. G. Gray, and B. A. Schrefler. A continuum mechanical framework for modeling tumor growth and treatment in two- and three-phase systems. *Archives of Applied Mechanics*, 2021. doi: 10.1007/s00419-021-01891-8.

[40] C. T. Miller, W. G. Gray, and B. A. Schrefler. A continuum mechanical framework for modeling tumor growth and treatment in two- and three-phase systems. *Archive of Applied Mechanics*, 92(2):461–489, 2022. doi: 10.1007/s00419-021-01891-8.

[41] C. T. Miller, W. G. Gray, C. E. Kees, I. V. Rybak, and B. J. Shepherd. Correction to: modelling sediment transport in three-phase surface water systems. *Journal of Hydraulic Research*, 61(1):168–171, 2023. doi: 10.1080/00221686.2022.2107580.

[42] W. Mmari and B. Johannesson. A model for multiphase moisture and heat transport below and above the saturation point of deformable and swelling wood fibers-II: Hygro-mechanical response. *Applications in Engineering Science*, 12:100118, 2022. doi: https://doi.org/10.1016/j.apples.2022.100118.

[43] I. Muller. *A History of Thermodynamics: The Doctrine of Energy and Entropy*. Springer Berlin / Heidelberg, Berlin, Heidelberg, 1 edition, 2007. doi: 10.1007/978-3-540-46227-9.

[44] T. N. Narasimhan. Fourier's heat conduction equation: History, influence, and connections. *Reviews of Geophysics*, 37(1):151–172, 1999.

[45] J. Niessner, S. Berg, and S. M. Hassanizadeh. Comparison of two-phase Darcy's Law with a thermodynamically consistent approach. *Transport in Porous Media*, 88:133–148, 2011. doi: 10.1007/s11242-011-9730-0.

[46] A. Q. Raeini, B. Bijeljic, and M. J. Blunt. Numerical modelling of sub-pore scale events in two-phase flow through porous media. *Transport in Porous Media*, 101(2):191–213, 2014.

[47] I. V. Rybak, W. G. Gray, and C. T. Miller. Modeling two-fluid-phase flow and species transport in porous media. *Journal of Hydrology*, 521:565–581, 2015. doi: 10.1016/j.jhydrol.2014.11.051.

[48] G. Sciumé, S. Shelton, W. G. Gray, C. T. Miller, F. Hussain, M. Ferrari, P. Decuzzi, and B. A. Schrefler. A multiphase model for three-dimensional tumor growth. *New Journal of Physics*, 15, 2013. doi: 10.1088/1367-2630/15/1/015005.

[49] C. Truesdell. *Rational Thermodynamics*. Springer, Berlin, 1984.

[50] I. Vavruch. Conceptual problems of modern irreversible thermodynamics. *Chemicke Listy*, 96(5):271–275, 2002.

[51] T. M. Weigand and C. T. Miller. Microscale modeling of nondilute flow and transport in porous medium systems. *Physical Review E*, 102(3), 2020. doi: 10.1103/physreve.102.033104.

[52] T. M. Weigand, P. B. Schultz, D. H. Giffen, M. W. Farthing, A. Crockett, C. T. Kelley, W. G. Gray, and C. T. Miller. Modeling nondilute species transport using the thermodynamically constrained averaging theory. *Water Resources Research*, 54(9):6656–6682, 2018.

[53] H. G. Weller, G. Tabor, H. Jasak, and C. Fureby. A tensorial approach to computational continuum mechanics using object-oriented techniques. *Comput. Phys.*, 12(6):620–631, 1998.

[54] S. Whitaker. *The Method of Volume Averaging*. Kluwer Academic Publishers, Dordrecht, 1999.

[55] L. Woods. More on the bogus axioms of continuum mechanics. *Bulletin of the Institute of Mathematics and Its Applications*, 18:64–67, 1982.

[56] L. C. Woods. Thermodynamic inequalities in continuum mechanics†. *IMA Journal of Applied Mathematics*, 29(3):221–246, 1982. doi: 10.1093/imamat/29.3.221.

[57] Y. Xia, A. Blumers, Z. Li, L. Luo, Y.-H. Tang, J. Kane, J. Goral, H. Huang, M. Deo, and M. Andrew. A GPU-accelerated package for simulation of flow in nanoporous source rocks with many-body dissipative particle dynamics. *Computer Physics Communications*, 247: 106874, 2020. doi: https://doi.org/10.1016/j.cpc.2019.106874.

[58] B. Zhao, C. W. MacMinn, B. K. Primkulov, Y. Chen, A. J. Valocchi, J. Zhao, Q. Kang, K. Bruning, J. E. McClure, C. T. Miller, A. Fakhari, D. Bolster, T. Hiller, M. Brinkman, L. Cueto-Felgueroso, D. A. Cogswell, R. Verma, M. Prodanović, J. Maes, S. Geiger, M. Vassvik, A. Hansen, E. Segre, R. Holtzman, Z. Yang, C. Yuan, B. Chareyre, and R. Juanes. Comprehensive comparison of pore-scale models for multiphase flow in porous media. *Proceedings of the National Academy of Sciences of the United States of America*, 116:13799–13806, 2019. doi: 10.1073/pnas.1901619116.

[59] Y. Zhao, P. K. Kumar, S. S. Sablani, and P. S. Takhar. Hybrid mixture theory-based modeling of transport of fluids, species, and heat in food biopolymers subjected to freeze–thaw cycles. *Journal of Food Science*, 87(9):4082–4106, 2022. doi: https://doi.org/10.1111/1750-3841.16279.